

Defects in yttrium aluminium perovskite and garnet crystals: atomistic study

This article has been downloaded from IOPscience. Please scroll down to see the full text article.

2000 J. Phys.: Condens. Matter 12 2953

(<http://iopscience.iop.org/0953-8984/12/13/307>)

View [the table of contents for this issue](#), or go to the [journal homepage](#) for more

Download details:

IP Address: 171.66.16.221

The article was downloaded on 16/05/2010 at 04:43

Please note that [terms and conditions apply](#).

Defects in yttrium aluminium perovskite and garnet crystals: atomistic study

Maija M Kuklja

Institute of Chemical Physics, University of Latvia, Riga, LV-1586, Latvia

and

Department of Electrical Engineering, Michigan Technological University, Houghton, MI, 49931-1295, USA

Received 21 September 1999, in final form 1 February 2000

Abstract. Native and impurity point defects in both yttrium aluminium perovskite (YAP) and garnet (YAG) crystals are studied in the framework of the pair-potential approximation coupled with the shell model description of the lattice ions. The calculated formation energies for native defects suggest that the antisite disorder is preferred over the Frenkel and Schottky-like disorder in both YAP and YAG. The calculated values of the distortion caused by the antisite Y_{Al}^x in the lattice turn out to be in an excellent agreement with the EXAFS measurements. In non-stoichiometric compounds, the calculated reaction energies indicate that excess Y_2O_3 or Al_2O_3 is most likely to be accommodated by the formation of antisites rather than vacancies or interstitials in the lattice. Enthalpies of the reactions for impurity (Ca^{2+} , Mg^{2+} , Sr^{2+} , Ba^{2+} , Cr^{3+} , Fe^{3+} , Nd^{3+} , Si^{4+}) incorporation into both YAP and YAG lattices are calculated. The relevant experimental data are discussed.

1. Introduction

Yttrium aluminium compounds, perovskite (YAP) and garnet (YAG), are important materials, of which the technological applications range from lasers to propulsion systems. It is well known that defects appearing in solids during crystal growth and under various external stimuli affect the structure and properties of the host material in different ways [1–3]. For example, the Nd^{3+} doped YAP and YAG are well known solid state laser crystals whereas the YAG: Al_2O_3 composite is found to be an ideal material for high-temperature structural ceramic applications [4]. Cr^{3+} codoping ions are often added to Nd^{3+} lasing ions in $YAlO_3$ crystals for an improvement of the pumping efficiency. Due to the disorder present in the host lattice, some processes governed by lattice and/or impurity defects (for example, the mechanism of the energy transfer, colour centres formation etc) are still not completely understood. Therefore, knowledge of the nature of intrinsic defects, defect distributions and interactions, and site preferences for impurity ions are of great importance.

Experimental studies of garnets started long ago since the garnet structure was originally solved by Menzer [5, 6]. The garnet structure belongs to the space group $Ia3d$ (O_h^{10}). The cations are all in special lattice positions labelled as a, c, d with no positional degrees of freedom, while the oxygen atoms are placed in the general positions 96(h). Yttrium occupies dodecahedral 24(c) positions whereas there are two different sites for aluminium ions, namely octahedral 16(a) and tetrahedral 24(d) in the lattice [7]. This leads to the formula of $Y_3Al_2Al_3O_{12}$, which is commonly written as $Y_3Al_5O_{12}$. The unit cell is quite large and

consists of eight formula units (160 atoms). For calculations, the oxygen positional parameters in the lattice were taken from neutron diffraction measurements ($x = -0.029$, $y = 0.053$ and $z = 0.151$) [8]. The x-ray diffraction study reports the cation–oxygen distances in YAG to be 1.94 Å and 1.76 Å for $\text{Al}^{3+}(\text{a})\text{--O}^{2-}$ and $\text{Al}^{3+}(\text{d})\text{--O}^{2-}$, respectively [9]. The most accurate value of the lattice constant for the stoichiometric $\text{Y}_3\text{Al}_5\text{O}_{12}$ is 12.000 ± 0.002 Å [10]. Several other experimental studies find the lattice constant to be slightly higher, which may be due to the presence of excess yttrium in the lattice [11].

There are several possible crystalline structures of YAIO_3 [7]. We have considered here YAP with the structure, which consists of four distorted perovskite pseudo-cells in an orthorhombic cell with the space group being $\text{D}_{2\text{h}}^{16}\text{--Pbnm}$ [12, 13]. The lattice constants are $a = 5.179$ Å, $b = 5.329$ Å and $c = 7.370$ Å.

Over the years, most of the experimental efforts have been focused on understanding the optical [14–18] and magnetic [19–22] properties of dopant ions in the YAG lattice. Relatively less attention has been paid to investigate its properties related to the high-temperature applications [23–25]. Diffusion and defect chemistry of pure and doped YAG have been a subject of a few experimental and theoretical studies [15, 26–30]. An analysis of electrical conductivity measurements and diffusion coefficients on a series of crystals with the garnet structure has established that YAG is an ionic conductor [26]. However, at high temperatures the situation changes and, as has been suggested, the YAG conductivity exhibits mixed ionic–electronic character for temperatures greater than 800 °C. A similar conclusion was also achieved from the study of transport properties and defect formation of Ca- and Mg-doped YAG [28].

A theoretical study based on the shell model has only considered the presence of vacancies and interstitials in the lattice predicting the dominance of vacancies over interstitials [29]. However, spectroscopic study of stoichiometry deviation in YAG has shown a possibility of cation antisite substitution in the garnet crystal lattice [31]. This has been confirmed recently by the EXAFS measurements in Y_2O_3 -rich YAG identifying the local order around the yttrium antisite atoms [32]. Furthermore, the atomistic study of the defects in yttrium iron garnet (YIG) has also concluded that antisites, not vacancies, will dominate the intrinsic disorder in this material [33]. Despite many experimental studies on YAIO_3 (see, for example, [34–38]) this compound has barely been investigated theoretically.

Due to a close similarity between YAG and YIG materials, it is therefore expected that antisites are likely to play an important role in YAG. On the other hand, YAIO_3 is constituted of the same chemical elements as YAG. This gives us grounds to assume that some common features of defect chemistry in YAG and YAP should appear.

In this paper, we seek to perform such a task reporting the results of a theoretical study of native and impurity defects in both YAP and YAG. Our approach is based on the pair-potential and shell model description of the ionic interactions in the crystalline lattice. Intrinsic and impurity disorder and reactions describing deviations from stoichiometry in the compounds are discussed in detail.

2. Method

The pair-potential model used in the present work is well described elsewhere [39–42]. For ionic materials interatomic potentials are in the form of a Buckingham potential [43]:

$$\phi_{ij}(r_{ij}) = A_{ij} \exp(-r_{ij}/\rho_{ij}) - C_{ij}/r_{ij}^6 \quad (2.1)$$

A_{ij} , ρ_{ij} and C_{ij} are short-range empirical parameters, that are usually fitted to crystalline properties. The short-range forces reflect the effect of electron cloud overlap and dispersion. In order to model dielectric properties and the long-range polarization energy for defects, a

Table 1. Interatomic potentials and shell constants. A and ρ are parameters in the equation for the Buckingham potential; Y^+ is the charge of the core; K^+ is the core-shell spring constant; C , the attractive contribution, for oxygen is $27.88 \text{ eV } \text{\AA}^{-6}$.

Ion	A (eV)	ρ (Å)	Y^+ ($ e $)	K^+ (eV Å ⁻²)
O ²⁻ -O ²⁻	22 764.000	0.149	0.8481	74.92
Y ³⁺ -O ²⁻	2036.8379	0.3103	-0.251	46.7288
Al ³⁺ -O ²⁻	741.9007	0.3566	0.043	40.8618
Ca ²⁺ -O ²⁻	1090.100	0.3437	-1.135	110.20
Mg ²⁺ -O ²⁻	946.627	0.318 13	2.0	—
Str ²⁺ -O ²⁻	950.1	0.3736	-1.35	63.25
Ba ²⁺ -O ²⁻	782.1	0.4084	-4.01	157.52
Cl ³⁺ -O ²⁻	1734.1	0.301	2.03	67.00
Fe ³⁺ -O ²⁻	1102.4	0.3299	-1.97	304.7
Nd ³⁺ -O ²⁻	1529.9	0.3601	3.0	—
Si ⁴⁺ -O ²⁻	913.2	0.3428	4.0	—

dipolar shell model of Dick and Overhauser [44] may be included. Here a massless charged *shell*, on which all pair potentials act, is coupled by an harmonic force to a *core* from which it is Coulombically screened:

$$E_{(core-shell)} = \frac{1}{2}k_{(core-shell)}r^2 \quad (2.2)$$

yielding an ion polarizability

$$\alpha_i = q_{shell}^2 / (k_{(core-shell)} + f_{shell}) \quad (2.3)$$

where q_{shell} is the shell charge, $k_{core-shell}$ represents the restoring force between the core and the shell and f_{shell} represents the completing distorting force due to the presence of the surrounding ions. Both shell and core charges and coupling constants of a shell and a core of the given ion are the parameters of the theory and are generally empirically derived.

For this investigation, we used a new set of interatomic potentials developed earlier [45]. In our model, formal ionic charges are assigned to the host-lattice ions, thereby considering them as Y³⁺, Al³⁺ and O²⁻ in YAG. The short-range interaction terms considered in the model describe cation-oxygen and oxygen-oxygen interactions. The short-range interactions between cations are ignored as they generally become very small for large separations which are 2.99 Å for R(Y-Al(d)); 3.67 Å for R(Y-Y) and R(Al(d)-Al(d)) and 5.19 Å for R(Al(a)-Al(a)) in YAG.

The parameters used for the O²⁻-O²⁻ interactions were obtained from Hartree-Fock calculations of the interaction of two negative oxygen ions [39, 42, 46]. Since the accurate representation of ionic polarization of a crystalline lattice is known to be very important for defect modelling, we treat all constituent ions of YAG (i.e. Y³⁺, Al³⁺ and O²⁻) as polarizable ions in the lattice. Model parameters are then fitted to the experimentally known YAG crystal properties such as the structure, elastic and dielectric constants as accurately as possible. In doing this we used a 'relaxed' fitting procedure [47], i.e. for each evaluation of the sum of squares the structure is relaxed to zero strain and the difference between observed and calculated structural parameters is used in place of the derivatives. Lattice properties thus are evaluated at the relaxed geometry. (For details of the fitting procedure, see [47] and [48].) The obtained interatomic potentials for Y³⁺-O²⁻ and Al³⁺-O²⁻ are given in table 1. As it is seen from table 2, the model parameters reproduce the crystalline properties of YAG very well thus providing us a sound basis for extending the model to defect calculations.

Recently, Bush *et al* [49] have obtained a consistent set of pair potentials empirically fitted specifically to the experimentally measured lattice properties of crystal oxides including YAG. This set is in addition to the potential set used earlier by Schuh *et al* [29], which was fitted to

Table 2. The calculated properties of YAG.

Ref.	Cohesive energy (eV) per formula	Lattice parameters		Elastic constants (10^{11} dyn cm $^{-2}$)			Dielectric constants	
		a (Å)	ρ (g cm $^{-3}$)	C_{11}	C_{12}	C_{44}	ϵ_0	ϵ_∞
Exp. [10, 64, 65]	—	12.000	4.53	33.3	11.3	11.5	11.0	3.5
This study	−589.28	11.988	4.58	34.0	12.7	11.2	11.4	3.5
Schuh <i>et al</i> [29]	−602.50	12.002	4.53	39.5	13.5	11.7	8.1	2.9
Bush <i>et al</i> [49]	−601.17	12.143	4.40	33.0	16.5	13.1	16.2	4.0

Al₂O₃ and Y₂O₃ structure properties [39, 50]. Although these two sets of interatomic potentials yield good agreement with the experimental values of the lattice structure and elastic constants of YAG, they do not yield the low- and high-frequency dielectric constants correctly. In fact, the dielectric constants are overestimated by the first parameter set (16.2 and 4.0) and are underestimated by the second set (8.1 and 2.9) as compared to the experimental values of 11.0 and 3.5. This discrepancy may be due to the different description of cationic polarizabilities. Bush's set considers rigid Y and polarizable Al and, in contrast, Schuh's set contains rigid Al and polarizable Y. On the basis of ionic radii, the Y ion is expected to be more polarizable than the Al one. From our calculations, inclusion of both Y and Al polarizabilities into the model allows us to describe dielectric properties of YAG very well. We note here that the accurate representation of the dielectric constants by the shell model is essential in obtaining reliable defect energies in ionic materials such as oxides. A detailed discussion on the results obtained on the basis of these three potential sets is provided [45].

It is to be noted here that the structure properties of oxides Y₂O₃, Al₂O₃, orthorhombic perovskite-like YAIO₃ and the garnet Y₄Al₄O₁₂ compound are also well reproduced by our potential model. For example, the calculated lattice constants of YAIO₃ ($a = 5.104$ Å, $b = 5.260$ Å, $c = 7.648$ Å) are in a good agreement with the experimental data (5.179, 5.329, 7.370, respectively [12, 13]). For the cubic Y₄Al₄O₁₂ the calculated lattice constant of 12.106 Å is only 0.9% larger than the experimental value of 11.989 Å [51].

To check further the adequacy of the derived potential parameters, we examine the stability of the lattices with respect to their component oxides:



The reaction enthalpies come out to be -2.4 eV (equation (2.4)) and -1.6 eV (equation (2.5)), respectively, per YAG formula unit indicating that YAG is indeed a stable compound. These values could be compared with the corresponding reaction enthalpies for YIG that are -1.6 eV and -2.9 eV, respectively [33]. For YAP, the enthalpy of the reaction (2.6) is -0.05 eV per formula unit.

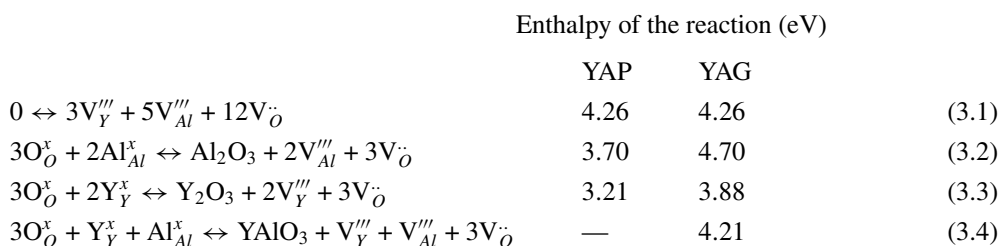
3. Results and discussion

3.1. Intrinsic defect structure

For calculations of native point defects, the lattice was simulated by large clusters, which contained more than 250 ions. The ions surrounding the defect in the cluster were allowed to relax until a minimum of the total energy was achieved. For an outer region, displacements of ions are determined by the electric field due to the effective charge of the defect in the

framework of the Mott–Littleton approximation [52]. The calculations were performed using the GULP (General Utility Lattice Program) code [48].

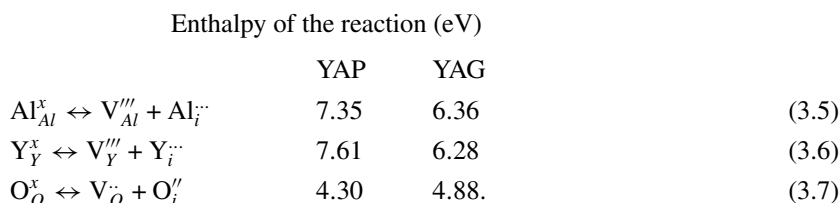
The calculated formation energies for the isolated basic defects (which are collected in appendix table A1) can now be used to analyse the energetics of Schottky and Frenkel disorder in the lattices. In the case of oxygen interstitials we probed all the possible positions in YAG, which are referred to as f and g [6]. For cations, the b positions were examined. For YAP, an empty a position was used for interstitials in accord with *Pbnm* symmetry. Since both YAP and YAG are complex oxides and their lattices consist of three sublattices, the possible Schottky-like structure disorder can be written in the form:



where we use the standard notations of Kröger and Vink [53] for defects.

Here, the reaction (3.1) corresponds to the true Schottky disorder and the remaining reactions (3.2)–(3.4) are given as examples of a change in the chemical composition of the material. They can be interpreted as a possibility of self-segregation in the stoichiometric crystals by the Schottky-like disorder in either of the cation sublattices.

The Frenkel disorder can be written as follows:



The computed formation energies suggest that the Schottky-like disorder appears to be more favourable than the Frenkel disorder. Nevertheless, even Schottky defect formation demands rather high energy (of about 3.9–4.7 eV per defect in YAG, and 3.2–4.2 eV per defect in YAP). Therefore, we can suppose that both Frenkel and Schottky defects are not likely to occur in these solids. This conclusion is in agreement with the results that have been reported for yttrium iron garnet (YIG) crystals [33]. Furthermore, large enthalpies of the reactions (3.2)–(3.4) preclude the occurrence of self-segregation in the stoichiometric crystals as also observed experimentally.

Next we consider antisite disorder in the cation sublattices, which can be described as follows:



The corresponding antisite-pair formation energy in YAG is estimated to be about 0.9 eV and 1.8 eV per defect for the reactions, (3.8) and (3.9), respectively. We note here that Y prefers to be located at the Al(a) site over the Al(d) site. This is expected on the basis of the coordination numbers of these ions in the lattice: Y has a coordination number of eight whereas Al(a)

and Al(d) ions have six and four nearest-neighbour oxygen ions, respectively. Antisite pair formation in the perovskite-like compound, $YAlO_3$ also requires a very low energy, which comes out to be 0.62 eV per defect. From this, we conclude that the antisite disorder is preferred over both Schottky and Frenkel disorder in both YAP and YAG, suggesting that these defects play an important role in the materials.

Experimental studies have in fact established that Y can occupy its regular dodecahedral sites as well as the Al(a) site in YAG [31]. The authors investigated non-stoichiometric $Y_3Y_xAl_{2-x}Al_3O_{12}$ crystals by measuring the spectra of rare-earth impurity ions in the lattice and have concluded that the substitution of Y at the Al(a) site introduces the lattice distortion. Recent XANES and EXAFS measurements [32] have investigated the local order around yttrium regular and antisite locations in Y_2O_3 rich YAG. As was shown, an increase of the electronegativity of the site ions after the substitution of Al cations by Y implies that the oxygen bond in the lattice becomes less ionic. This results in the shortening of the distance between Y and O from $R(Y-O) = 2.43 \text{ \AA}$ to $R(Y-O) = 2.10 \text{ \AA}$. This new shortened distance is now close to the mean distance $R(Y-O)$ of yttrium in octahedral position in yttria (Y_2O_3). From our calculation, the substitution of Y at the Al(a) site in YAG lattice is accompanied by the decrease of the distance $R(Y-O)$ to 2.08 \AA , which is in excellent agreement with the experimental value of 2.10 \AA .

3.2. Deviations from stoichiometry

Although experimental studies have long ago identified the presence of non-stoichiometric phases in yttrium aluminium compounds, the mechanisms by which an excess of yttria or alumina can be accommodated in the lattices are not completely understood. In the early work on gallium and aluminium garnets [11], excess of yttrium oxide was found to be soluble in the garnet. Geller [10] discussed a possible mechanism of the solid solution in the garnet structure, which may involve a vacancy or vacancy–interstitial complex instead of substitutional atoms. Neiman *et al* [26] reported that the YAG structure can exist with some deficit of Al_2O_3 . Several studies have also identified Al_2O_3 inclusions in YAG ceramics [54, 55]. In this study, we aim to find the most probable mechanisms of accommodating the deviations from stoichiometry in both YAP and YAG structures.

For Y_2O_3 excess, we collect the equations involving the formation of vacancies, interstitials and antisites with the calculated enthalpies of the reactions in table 3. Quite similarly we can describe the accommodation of excess of Al_2O_3 the calculated results of which are listed in table 4. Inspecting the list of the reactions and energies for YAG, we notice that two reactions, (3.13) and (3.16), have negative energies and are therefore exothermic. This leads to the conclusion that the antisite substitution of $Y_{Al(a)}^x$ is the most favourable of all the possible mechanisms of accommodation of extra Y ions in YAG structure. X-ray microscope studies on YAG ceramics observed precipitates, which were identified as YAP in the Y_2O_3 excess specimens [56]. In our study, the same proposal is expected from the equation (3.13), which describes perovskite phase and antisite formation. Moreover, by analysing the energies of the mentioned reactions, one can predict an existence of a reversible YAP–YAG phase transition, which was indeed observed by differential scanning calorimetry [57]. The energies of the equations (3.13) and (3.16) can be compared with the energy of the reaction (3.10), which describes antisite Y_{Al}^x formation accompanied by segregation of Al_2O_3 and shows a very small (endothermic) enthalpy of the reaction indicating a high probability of its occurrence. Alumina inclusion formations as well as the perovskite phase may therefore be stimulated by yttria surplus in YAG. A deficit of alumina in the garnet structure as postulated by Neiman *et al* [26], indeed can exist in YAG. YAP exhibits a similar trend showing an antisite

Table 3. Y₂O₃ excess in YAP and YAG crystals.

No	Mechanism	Energy of the reaction (eV)	
		YAP	YAG
(3.10)	$Y_2O_3 + 2Al_{Al(a)}^x \leftrightarrow 2Y_{Al(a)}^x + Al_2O_3$	1.0	0.5
(3.11)	$Y_2O_3 \leftrightarrow 2Y_i''' + 3O_i''$	40.2	36.2
(3.12)	$Y_2O_3 + 2Al_{Al(a)}^x + 3O_O^x \leftrightarrow 2YAlO_3 + 2V_{Al(a)}''' + 3V_O^\cdot$	18.0	23.3
(3.13)	$Y_2O_3 + Al_{Al}^x \leftrightarrow YAlO_3 + Y_{Al}^x$	0.25	-0.02
(3.14)	$Y_2O_3 + Al_{Al}^x \leftrightarrow YAlO_3 + Y_i''' + V_{Al}'''$	16.2	14.2
(3.15)	$Y_2O_3 + \frac{2}{3}Al_{Al(a)}^x + O_O^x \leftrightarrow \frac{1}{3}Y_3Al_5O_{12} + Y_{Al(a)}^x + \frac{2}{3}V_{Al(a)}''' + V_O^\cdot$	5.9	7.4
(3.16)	$Y_2O_3 + \frac{1}{2}Al_{Al(a)}^x + \frac{3}{4}Al_{Al(d)}^x \leftrightarrow \frac{1}{4}Y_3Al_5O_{12} + \frac{5}{4}Y_{Al(a)}^x$	0.04	-0.3
(3.17)	$Y_2O_3 + \frac{1}{2}Al_{Al(a)}^x + \frac{3}{4}Al_{Al(d)}^x \leftrightarrow \frac{1}{4}Y_3Al_5O_{12} + \frac{5}{4}Y_i''' + \frac{1}{2}V_{Al(a)}''' + \frac{3}{4}V_{Al(d)}'''$	20.0	9.4
(3.18)	$Y_2O_3 + \frac{4}{3}Al_{Al(a)}^x + 2Al_{Al(d)}^x + 5O_O^x \leftrightarrow \frac{2}{3}Y_3Al_5O_{12} + \frac{4}{3}V_{Al(a)}''' + 2V_{Al(d)}''' + 5V_O^\cdot$	29.3	38.1

Table 4. Al₂O₃ excess in YAP and YAG crystals.

No	Mechanism	Energy of the reaction (eV)	
		YAP	YAG
(3.20)	$Al_2O_3 + 2Y_Y^x \leftrightarrow 2Al_Y^x + Y_2O_3$	1.5	2.9
(3.21)	$Al_2O_3 \leftrightarrow 2Al_i''' + 3O_i''$	36.6	52.2
(3.22)	$Al_2O_3 + 2Y_Y^x + 3O_O^x \leftrightarrow 2YAlO_3 + 2V_Y''' + 3V_O^\cdot$	15.6	18.9
(3.23)	$Al_2O_3 + Y_Y^x \leftrightarrow YAlO_3 + Al_Y^x$	0.5	1.2
(3.24)	$Al_2O_3 + Y_Y^x \leftrightarrow YAlO_3 + Al_i''' + V_Y'''$	13.2	10.6
(3.25)	$Al_2O_3 + Y_Y^x + O_O^x \leftrightarrow \frac{1}{3}Y_3Al_5O_{12} + \frac{1}{3}Al_Y^x + \frac{2}{3}V_Y''' + V_O^\cdot$	3.9	5.7
(3.26)	$Al_2O_3 + \frac{3}{4}Y_Y^x \leftrightarrow \frac{1}{4}Y_3Al_5O_{12} + \frac{3}{4}Al_Y^x$	-0.7	0.2
(3.27)	$Al_2O_3 + \frac{3}{4}Y_Y^x \leftrightarrow \frac{1}{4}Y_3Al_5O_{12} + \frac{3}{4}Al_i''' + \frac{3}{4}V_Y'''$	9.5	7.6
(3.28)	$Al_2O_3 + \frac{6}{5}Y_Y^x + \frac{9}{5}O_O^x \leftrightarrow \frac{2}{5}Y_3Al_5O_{12} + \frac{6}{5}V_Y''' + \frac{9}{5}V_O^\cdot$	8.7	10.7

substitution preference over all other mechanisms for yttria excess accommodation in the YAP lattice. Comparing the energies of the reactions (3.16) and (3.26), we find that the $Y_{Al(a)}^x$ antisite formation in Y₂O₃ rich YAG is slightly preferable over the formation of Al_Y^x in Al₂O₃ rich YAG although the latter is still possible due to the small enthalpy of the process. Besides, these reactions indicate that extra Y ions can be accommodated in the YAG lattice more easily than Al ions. This fact is known from experiments. For example, an excess of Y₂O₃ up to 2% was reported while a surplus of Al₂O₃ in YAG was seen only up to 0.5% (see, for instance, [30]). In contrast, segregation of YAG phase accompanied by Al_Y^x antisite formation in alumina rich perovskite is the most favourable (exothermic) reaction for YAP (equation (3.26)). This is supported by the conclusion drawn from equation (2.5) stressing that YAG may be formed from YAP and alumina. In other words, Al₂O₃ excess in YAlO₃ will cause garnet structure growth. Quite opposite to YAG, perovskite prefers an excess of aluminium ions to be situated in the lattice instead of yttrium ions.

The formation of defect complexes like an interstitial and the corresponding vacancy (see the reactions (3.14), (3.17) and (3.24), (3.27)) requires much more energy with respect to the antisite formation (the reactions (3.13), (3.16) and (3.23), (3.26), respectively). The required energies for the formation of interstitial defects, described by the reactions (3.11) and (3.21), are also very high as was expected from Frenkel disorder energetics. The segregation in the perovskite-like phase (reactions (3.12) and (3.22)) with complementary cation and anion

vacancy formation in YAG is also expected to have a low probability due to very high energy of the reaction.

The reaction (3.15) represents a mechanism of the defect accommodation predicted by Neiman *et al* [26] while equation (3.25) is composed by analogy. The reactions (3.18) and (3.28) describe the process suggested by Sakaguchi *et al* [30]. From our calculations, both of these mechanisms are not predicted to take place in the YAG crystal. The calculated results imply that the defect equilibrium in an excess material has a different nature than that considered in these studies. Excess of neither Y_2O_3 nor Al_2O_3 appears to be a source of oxygen vacancies in both pure compounds YAP and YAG. It should be noted here that an interaction between defects, that may be important under the conditions of large deviations from stoichiometry in materials, was not included in the present study.

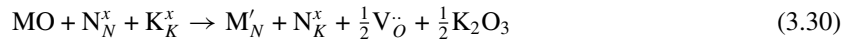
3.3. Impurity defects

As mentioned above, the garnet crystals have complex three-sublattice structure that allows almost all periodic-system elements to be incorporated in the crystal. The crystal with an extrinsic defect was simulated by a large 270–320-ions cluster in which one regular lattice cation is substituted by an impurity ion.

3.3.1. Divalent impurities. First, we consider most common impurity defects in YAG and YAP crystals. Here, a divalent substitution ion represents a point defect negatively charged with respect to the crystal lattice. The process of such kind of defect formation should be accompanied by a charge compensation. The possible mechanisms are listed below.



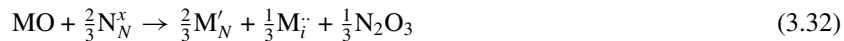
where M denotes impurity ion (in our case, they are Ca^{2+} , Mg^{2+} , Sr^{2+} , Ba^{2+}) and N is a host ion (for YAG, they are Y^{3+} , $Al(a)^{3+}$, $Al(d)^{3+}$). In these notations M'_N indicates a single charged defect, which is a metal impurity in the cation lattice site.



(M = metal impurity ion; N = Y^{3+} , $Al(a)^{3+}$ and K = $Al(a)^{3+}$, Y^{3+}).



N indicates again each of the host ions.



the subscript *i* denotes an interstitial M ion, which is placed into empty b position in the YAG lattice. Equation (3.29) represents the oxygen vacancy charge compensation mechanism. It is well established theoretically and experimentally that the anion vacancy compensation provides the lowest energy in garnets since disorder in the oxygen sublattice is the most favourable energetically [26, 29]. Reaction (3.30) describes the same mechanism with cation antisite defect formation in addition. Cation interstitial formation as a result of impurity substitution is taken into account in equation (3.31). The last reaction (3.32) corresponds to self-compensation, i.e., for example, a high Mg-dopant level may arrange impurity accommodation in both a regular lattice site and in an interstitial position as well. The corresponding solution enthalpies are listed in tables 5–8, respectively.

From our calculations, an oxygen vacancy charge compensation mechanism is the most favourable for YAP, as was expected. In accord with table 5, Mg^{2+} ion is able to substitute both Y and Al sites in the YAP lattice with an approximately similar value of the solution enthalpy. Three other studied impurities prefer to occupy the Y site. The most probable mechanism for

Table 5. Solution enthalpies of the reactions for divalent impurities for oxygen vacancy compensation mechanism: $MO + N_N^x \rightarrow M'_N + \frac{1}{2}V''_O + \frac{1}{2}N_2O_3$. Enthalpies of the reactions are given in eV.

Impurity (M)	Cation site in YAP lattice (N)		Cation site in YAG lattice (N)		
	Al	Y	Al(a)	Al(d)	Y
Ca	3.9	1.9	3.7	4.5	2.1
Mg	2.3	2.1	2.7	2.9	2.8
Sr	5.9	2.9	5.2	6.2	2.9
Ba	8.6	4.8	7.2	8.3	4.6

Table 6. Solution enthalpies of the reactions for divalent impurities for the oxygen vacancy compensation mechanism and antisite formation in addition: $MO + N_N^x + K_K^x \rightarrow M'_N + N_K^x + \frac{1}{2}V''_O + \frac{1}{2}K_2O_3$.

Impurity (M)	Cation site in YAP lattice (N)		Cation site in YAG lattice (N)		
	Al	Y	Al(a)	Al(d)	Y
Ca	4.7	2.4	5.2	6.0	2.3
Mg	3.0	2.6	4.2	4.4	3.0
Sr	6.7	3.4	6.6	7.6	3.1
Ba	9.3	5.3	8.6	9.7	4.8

Table 7. Solution enthalpies of the reactions for divalent impurities for the interstitial compensation mechanism: $MO + N_N^x \rightarrow M'_N + \frac{1}{3}N_i''' + \frac{1}{3}N_2O_3$.

Impurity (M)	Cation site in YAP lattice (N)		Cation site in YAG lattice (N)		
	Al	Y	Al(a)	Al(d)	Y
Ca	5.7	4.3	4.1	4.9	3.1
Mg	4.1	4.5	3.1	3.3	3.7
Sr	7.7	5.3	5.6	6.6	3.9
Ba	10.4	7.2	7.6	8.7	5.5

Table 8. Solution enthalpies of the reactions for divalent impurities for the interstitial self-compensation mechanism: $MO + \frac{2}{3}N_N^x \rightarrow \frac{2}{3}M'_N + \frac{1}{3}M''_i + \frac{1}{3}N_2O_3$.

Impurity (M)	Cation site in YAP lattice (N)		Cation site in YAG lattice (N)		
	Al	Y	Al(a)	Al(d)	Y
Ca	5.2	3.9	4.0	4.5	2.9
Mg	3.1	3.0	2.2	2.3	2.2
Sr	7.3	5.3	5.9	6.6	4.4
Ba	10.0	7.4	8.4	9.1	6.6

oxide solid solutions in YAG is again the oxygen vacancy compensation mechanism. However, further Y_{Al}^x antisite formation requires almost the same low energy for Ca^{2+} and Sr^{2+} cases (table 6). Therefore, a high concentration of anion vacancies and antisites is predicted to occur for Ca^{2+} and Sr^{2+} doped YAG. An exception is the Mg^{2+} impurity in YAG, which turned out to

Table 9. The binding energies for the defect complexes in YAG.

Impurity	The binding energy of the defect complex (in eV)		
	$(M'_Y + V''_O)'-(1NN)$	$(M'_Y + V''_O)'-(2NN)$	$(2M'_Y + V''_O)$
Ca	0.94	0.54	2.17
Mg	1.20	0.69	2.23
Sr	1.06	0.47	2.26
Ba	1.42	0.58	2.46

be incorporated in the YAG lattice not only via the oxygen vacancy compensation but also via the self-compensation mechanism, occupying any possible cation site and an empty interstitial position (table 8). There is a strong correlation between an ionic radii of the impurities and the solution enthalpy of the corresponding oxide in both perovskite or garnet lattices.

The enthalpy of solution can be further reduced due to a defect clustering effect [58, 59]. Therefore, we have studied positively charged complexes $(M'_Y + V''_O)'$, calculating binding energies for both the nearest (1NN) and the second (2NN) pairs of defects in YAG. The obtained data are collected in table 9. The corresponding energies were obtained by the formula:

$$E_{binding} = E(M'_Y) + E(V''_O) - E[(M'_Y + V''_O)'] \quad (3.33)$$

where $E[(M'_Y + V''_O)']$ is the complex formation energy, $E(M'_Y)$ is a substitutional defect formation energy and $E(V''_O)$ is the oxygen vacancy formation energy. From table 9, the nearest pair of defects is preferable over an isolated pair, and the binding energies are higher for the nearest pair of defects than for the second pair for all impurities.

Furthermore, calculations of binding energies for the nearest three defects, which represent neutral complexes, were performed. The corresponding data (table 9) were obtained using an expression:

$$E_{binding} = 2E(M'_Y) + E(V''_O) - E(2M'_Y + V''_O). \quad (3.34)$$

A comparison of the latter with the data for the charged complexes indicates that the neutral complexes are the most favourable. This is expected on the basis of Coulombic interactions between charged defects. We can conclude from our results that the divalent impurities tend to form precipitates in the garnet structure, which should be located near oxygen vacancies. This deduction is also supported by experimental investigations [18, 28]. Clearly, the binding between the cation impurity and anion vacancies should cause changes in oxygen diffusion behaviour precluding movement, which was actually observed in ionic conductivity measurements [15, 26, 28]. As was discussed, the activation energy for oxygen diffusion in YAG becomes almost twice as high for heavily doped Ca:YAG as for the undoped crystal [15]. In fact, the energy of association of the complex $(Ca'_Y + V''_O)'$ is estimated as 1.7 eV [60] to fall into the range of our results for the nearest pair (0.94 eV) and the nearest trio of defects (2.17 eV). Taking into account that there is a non-uniform distribution of defects in real crystals, and the experimental result gives us averaged data, the obtained agreement is to be considered as reasonable. It should be concluded that divalent impurities try to be placed near an oxygen vacancy forming neutral aggregates in the garnet crystal lattice.

3.3.2. Trivalent impurities. A trivalent impurity represents a neutral defect with respect to the lattice and is the simplest since it does not need any charge compensation. Therefore, the impurity solution mechanism is described by the reaction:



Table 10. Solution enthalpies (in eV) of the reactions for trivalent impurities: $M_2O_3 + 2N_N^x \rightarrow 2M_N^x + N_2O_3$.

Impurity (M)	Cation site in YAP lattice (N)		Cation site in YAG lattice (N)		
	Al	Y	Al(a)	Al(d)	Y
Fe	0.09	1.61	0.07	1.39	2.71
Cr	0.05	1.77	0.09	2.41	3.07
Nd	7.41	1.71	5.29	8.83	0.89

M indicates here a trivalent impurity ion, and N is one of the possible host cations. The corresponding solution enthalpies of the reactions for Fe^{3+} , Cr^{3+} , and Nd^{3+} are collected in table 10. As observed, trivalent impurities have low solution energies, meaning a noticeable concentration of these dopants can be created in both YAP and YAG crystals. The Fe^{3+} ion prefers occupy the Al site in YAP and the Al(a) site in YAG, although its substitution into the Al(d) site has a rather low energy that makes this accommodation possible, too. In fact, a similar site preference of Fe^{3+} ions in YAG was reported [61, 62]. The possible distribution of Fe^{3+} between the sites in YAG is also discussed [61].

Cr_2O_3 solubility in both YAP and YAG is also high. Cr^{3+} prefers an Al position in the YAP lattice and an Al(a) site in YAG. The experimental evidence of Cr^{3+} ions entering only octahedral sites of the garnet lattice was examined [18, 19, 62]. For our calculations, we have neglected crystal-field corrections for open shell ions. The estimated corrections for the Cr^{3+} ion in the Fe^{3+} (a) site for YIG crystals demonstrate that the corresponding energy term gives a small contribution to the site stabilization energy though it does not change the obtained results in general [63].

Compared to Fe^{3+} and Cr^{3+} , which are placed in Al sites, Nd^{3+} enters the Y position due to its large ionic radius. Moreover, Nd^{3+} is more soluble in the garnet structure than in the perovskite lattice. A similar trend is obtained in the YIG crystal where small impurities prefer to occupy the Al(a) site and large ions substitute the Y(c) site [63]. This conclusion, which is common for the studied crystals (YAG and YIG), is indeed what we should expect because of the close similarity of the YAG and YIG crystal-chemical structures. In fact, YAG differs from YIG by replacing aluminium by iron ions in the same crystal lattice with the garnet structure. This causes significant changes in electronic disorder and not influence visibly the nature of the dominant atom defect formations [26].

The high solubility of Fe_2O_3 in YAG, which is determined by the very low energy of the reaction, results in a continuous series of $Y_3Fe_xAl_{5-x}O_{12}$ compounds with the garnet structure. Thus, YAG can be gradually transformed into YIG. Iron at all levels in YAG–YIG solid solutions had a major effect on the electrical and optical properties of the crystals [61]. From our calculations, we predict this property to take place also for Cr_2O_3 solutions in both YAP and YAG crystals.

3.3.3. Tetravalent impurities. We consider the Si^{4+} ion as an example of a tetravalent impurity, i.e. a single positively charged defect with respect to the lattice. We note here that Si^{4+} prefers to be accommodated in the Al site in the YAP lattice and in the Al(d) position in YAG crystals. The solution reactions with the possible mechanisms of charge compensation are shown in table 11. The reaction (3.36) represents a combined oxygen and cation vacancy charge compensation mechanism while the next three equations (3.37)–(3.39) describe the pure cation vacancy mechanism. The reactions notify formation of the complementary cation vacancy and the perovskite-like (3.38) or the garnet-like (3.39) compound phase aggregation in

Table 11. SiO₂ solubility mechanisms in YAP and YAG crystals.

No	Mechanism	Energy of the reaction (eV)	
		YAP	YAG
(3.36)	$\text{SiO}_2 + \frac{4}{3}\text{Al}_{Al}^x \leftrightarrow \text{Si}_{Al} + \text{V}_{\text{O}}^{\cdot\cdot} + \text{V}_{Al}^{\prime\prime} + \frac{2}{3}\text{Al}_2\text{O}_3$	7.4	8.7
(3.37)	$\text{SiO}_2 + \frac{4}{3}\text{Al}_{Al}^x \leftrightarrow \text{Si}_{Al} + \frac{1}{3}\text{V}_{Al}^{\prime\prime} + \frac{2}{3}\text{Al}_2\text{O}_3$	1.2	1.0
(3.38)	$\text{SiO}_2 + \text{Al}_{Al}^x + \frac{1}{3}\text{Y}_Y^x \leftrightarrow \text{Si}_{Al} + \frac{1}{3}\text{V}_Y^{\prime\prime} + \frac{1}{3}\text{YAlO}_3 + \frac{1}{3}\text{Al}_2\text{O}_3$	0.7	0.3
(3.39)	$\text{SiO}_2 + \frac{5}{6}\text{Al}_{Al}^x + \frac{1}{2}\text{Y}_Y^x \leftrightarrow \text{Si}_{Al} + \frac{1}{3}\text{V}_Y^{\prime\prime} + \frac{1}{6}\text{Y}_3\text{Al}_5\text{O}_{12}$	0.8	0.4
(3.40)	$\text{SiO}_2 + \text{Al}_{Al}^x \leftrightarrow \text{Si}_{Al} + \frac{1}{2}\text{O}_i^{\prime\prime} + \frac{1}{2}\text{Al}_2\text{O}_3$	2.4	2.0
(3.41)	$\text{SiO}_2 + \text{Al}_{Al}^x + \text{Y}_Y^x \leftrightarrow \text{Si}_{Al} + \text{Al}_Y^x + \frac{1}{2}\text{O}_i^{\prime\prime} + \frac{1}{2}\text{Y}_2\text{O}_3$	3.1	3.5
(3.42)	$\text{SiO}_2 + \frac{4}{3}\text{Al}_{Al}^x + \text{Ca}_{Ca}^x \leftrightarrow \text{Si}_{Al} + \text{Ca}_{Al}^{\prime} + \frac{2}{3}\text{Al}_2\text{O}_3$	15.5	14.4
(3.43)	$\text{SiO}_2 + \frac{4}{3}\text{Y}_Y^x + \text{Ca}_{Ca}^x \leftrightarrow \text{Si}_Y^{\prime} + \text{Ca}_Y^{\prime} + \frac{2}{3}\text{Y}_2\text{O}_3$	13.9	16.5

addition. The most probable Si⁴⁺ incorporation in YAP and YAG lattices is associated with the cation vacancies. An appearance of oxygen vacancies in addition seems to have higher energy. An oxygen interstitial compensation, calculated by the reaction (3.40), also has a relatively low enthalpy of reaction. The next line (reaction (3.41)) describes the same mechanism accompanied by the antisite defect formation, which takes an extra 1–1.5 eV of energy. The last two equations (3.42) and (3.43) consider the self-compensation mechanism when both divalent and tetravalent impurities are present in the crystal. Both of them are unlikely to occur, either in YAP or YAG crystals. The calculated energies of the reactions for SiO₂ solutions may be also further reduced due to attractive interactions between charged defects, Si_{Al} and V_{Al}^{′′}.

Using our calculations, one may attempt to explain the experimental observations on silicon-rich garnet [30]. As was found, for Y₂O₃ excess specimens, there is a second phase (YAP) containing silicon and no silicon segregation at the grain boundary. For Al₂O₃ excess specimens, aluminium rich particles (alumina) and silicon rich segregant layers exist in the grain boundary. In terms of the solution energetics, we suggest the following interpretation. SiO₂ solid solution in yttrium aluminium garnet will proceed most likely under equations (3.38)–(3.39), which suggest co-existence of the YAG and YAP phases with some alumina inclusions. Yttrium vacancies formed as a result of this mechanism suggest that the Y₂O₃ excess can be easily arranged in these samples. Thus, the mentioned reactions coupled with either reactions (3.13) or (3.16) dictate Si ions are expected to be incorporated into Al sites of both YAP and YAG solid phases. On the other hand, equation (3.37), having a relatively high energy, can be thought of as favourable for the Al₂O₃ excess situation in the garnet structure. Combining it further with reaction (3.26), one can predict only a small fraction of Si ions to be accommodated in garnet lattice positions; the YAP solid phase is not likely to occur and plenty of alumina inclusions will be observed. One has to recall here that Al₂O₃ excess has significantly lower solubility in YAG than Y₂O₃ excess. This proves that both Si⁴⁺ and alumina must segregate on the surface or grain boundaries of the YAG samples. This also will affect oxygen diffusion observed [30].

4. Conclusions

In the present theoretical study, atomistic calculations of intrinsic and extrinsic point defects in both YAP and YAG crystals are performed. The Schottky and Frenkel defect formation energies are calculated as well as antisite substitutions in the cation sublattice. The calculated results allow us to make several important conclusions. Intrinsic disorder in both stoichiometric compounds (YAP and YAG) is dominated by antisites. An antisite substitution Y_{Al(a)}}^x causes a

distortion of the YAG crystalline lattice shortening the Y–O bond length; the calculated value is in excellent agreement with the EXAFS measurements. An excess of Y_2O_3 is the energetically more favourable with respect to Al_2O_3 surplus in YAG. The opposite situation is predicted to occur in YAP where Al extra ions can be easily accommodated in the lattice unlike extra Y ions. Formation of antisite disorder in both YAP and YAG with excess yttria or alumina is the most probable mechanism of accommodating the deviations from stoichiometry.

Solid solutions of divalent, trivalent and tetravalent impurities proceed in the compounds via different scenarios. The solution of the most divalent impurities favours an oxygen vacancy charge compensation mechanism for both YAP and YAG. The metal ions prefer to occupy the Y site in the lattice. Unlike others, MgO is soluble via both the oxygen vacancy and the self-compensation mechanism in YAG. Mg^{2+} ions can be located in any cation site and in an empty interstitial position in addition. The calculated enthalpies of the reactions are reduced due to defect cluster formation. Divalent impurities tend to be placed near oxygen vacancies forming neutral aggregates. Trivalent impurities have low solution enthalpies indicating high solubility in both YAP and YAG crystals. Fe^{3+} and Cr^{3+} ions are accommodated in Al sites, and Nd^{3+} prefers the Y position. SiO_2 , which has been simulated as an example of a tetravalent impurity, being easily soluble in YAG, stimulates the YAP phase aggregation accompanied by cation vacancies.

The calculated results are in good agreement with existing experimental data and allow us to suggest a consistent interpretation for observations.

Appendix

Table A1. Defect formation energies (eV) in YAP and YAG crystals.

Defect	YAP		YAG		
Cation vacancy					
V_{Al}	52.09		53.76 (Al(a)); 53.44 (Al(d))		
V_Y	48.70		49.42		
Oxygen vacancy V_O	20.90		21.54		
Interstitials					
Al_i	–37.40		–40.72		
Y_i	–33.48		–36.85		
O_i	–12.31		–11.38 ($O_i(g)$); –11.79 ($O_i(f)$)		
Antisites					
Y in Al site	2.65		2.38 ($Y_{Al(a)}$); 4.16 ($Y_{Al(d)}$)		
Al in Y site	–1.41		–0.69		
Impurities	In Al site	In Y site	In Al(a) site	In Al(d) site	In Y site
Ca	31.69	27.55	31.16	31.96	27.40
Mg	25.58	23.23	25.72	25.89	23.59
Sr	36.33	31.16	35.24	36.22	30.83
Ba	41.27	35.32	39.55	40.69	34.81
Cr	–2.95	–4.24	–2.93	–1.77	–3.59
Fe	–0.98	–2.37	–0.99	–0.33	–1.82
Nd	14.53	9.53	13.47	15.24	9.12
Si	–43.82	–44.15	–43.48	–44.46	–41.44

References

- [1] Catlow C R A 1997 *Computer Modelling in Inorganic Crystallography* (San Diego: Academic) p 340
- [2] Grimes R W, Catlow C R A, Shluger A L 1991 *Quantum Mechanical Cluster Calculations in Solid State Studies* (Singapore: World Scientific) p 470
- [3] Zakis Y R, Kantorovich L N, Kotomin E A, Kuzovkov V N, Tale I A and Shluger A L 1991 *Models of Processes in Wide-gap Solids with Defects* (Zinatne, Riga)
- [4] Parthasarathy T A, Mah T and Matson L E 1990 *Ceram. Eng. Sci. Proc.* **11** 1628
- [5] Menzer G 1926 Die Kristallstruktur von Granat *Z. Kristallogr.* **63** 157–8
- [6] Menzer G 1928 Die Kristallstruktur der Granate *Z. Kristallogr.* **69** 300–96
- [7] Wyckoff R W G 1965 *Crystal Structures* vol 1 (New York: Wiley) p 467
- [8] Prince E 1957 *Acta Crystall.* **10** 787–88
- [9] Euler F and Bruce J A 1965 *Acta Crystall.* **19** 971–8
- [10] Geller S 1967 *Z. Kristallogr.* **125** 1–47
- [11] Keith M Z and Roy R 1954 *Amer. Mineral.* **39** 1–23
- [12] Geller S and Wood E A 1956 *Acta Crystallogr.* **9** 563
- [13] Geller S and Bala V B 1956 *Acta Crystallogr.* **9** 1019
- [14] Kitaeva V F, Sobolev N N, Chistyj I L, Zharikov E V, Osiko V V, Timoshechkin M I and Zolot'ko A C 1980 *Sov. Solid State Phys.* **22** 1379
- [15] Rotman S R 1990 *Phys. Rev. B* **41** 791–2
- [16] Rotman S R, Tuller H L and Warde C 1992 *J. Appl. Phys.* **71** 1209–14
- [17] Rozenfeld Y B and Rotman S R 1993 *Phys. Status Solidi A* **139** 249–62
- [18] Sugimoto A, Nobe Y and Yamagishi K 1994 *J. Cryst. Growth* **140** 349–54
- [19] Vetrogon G I, Danilenko V I, Kabanchenko V Ya, Osiko V V, Prohorov A M, Terent'evskij A N and Timoshechkin M I 1980 *Sov. Solid State Phys.* **22** 3216
- [20] Massiot D, Bessada J P, Countures J P and Tauelle F 1990 *J. Magn. Reson.* **90** 231–42
- [21] Zhilyakov S M, Mal'cev V I and Naiden E P 1980 *Sov. Solid State Phys.* **22** 1388–93
- [22] Asatryan G R, Baranov G P and Zhekov V I 1996 *Sov. Solid State Phys.* **38** 814–21
- [23] Kumar J, Thirumavalavan M, Dhanasekaran R, Gnanam F D and Ramasamy P 1986 *J. Phys. D: Appl. Phys.* **19** 1223–31
- [24] Kim N H, Fun Q D, Komeya K and Meguro T 1996 *J. Am. Ceram. Soc.* **79** 2645–51
- [25] Blumenthal W R and Philips D S 1996 *J. Am. Ceram. Soc.* **79** 1047
- [26] Neiman A Ya, Tkachenko E V and Zhukovskii V M 1978 *Dokl. Akad. Nauk USSR* **240** 876–9
- [27] Haneda H, Miyazawa Y and Shirasaki S 1984 *J. Cryst. Growth* **68** 581–8
- [28] Schuh L, Metselaar R and de With G, 1989 *J. Appl. Phys.* **66** 2627
- [29] Schuh L, Metselaar R and Catlow C R A 1991 *J. Eur. Ceram. Soc.* **7** 67–74
- [30] Sakaguchi I, Haneda H and Tanaka J 1996 *J. Am. Ceram. Soc.* **79** 1627–32
- [31] Ashurov M Kh, Voronko Yu K, Osiko V V, Sobol A A and Timoshechkin M I 1977 *Phys. Status Solidi a* **42** 101
- [32] Landron C, Lefloch S, Gervais M, Countures J P and Bazin D 1996 *Phys. Status Solidi b* **196** 25
- [33] Donnerberg H and Catlow C R A 1993 *J. Phys.: Condens. Matter* **5** 2947
- [34] Rotman S R, Luria E, Mares J A, Boulon G, Brenier A and Lou L 1996 *J. Appl. Phys.* **80** 1094–8
- [35] Luria E, Rotman S R, Mares J A, Boulon G, Brenier A and Lou L 1997 *J. Lumin.* **72–74** 951–3
- [36] Wolfenstine J and Parthasarathy T A 1992 *Scr. Metall.* **26** 1649–53
- [37] Murk V, Kuznetsov A, Namazov B and Ismailov K 1994 *Nucl. Instrum. Methods B* **91** 327–30
- [38] Hong Hua and Vohra Y K 1997 *Appl. Phys. Lett.* **71** 2602–4
- [39] Catlow C R A and James R 1982 *Phys. Rev. B* **25** 1006–26
- [40] Lidiard A B and Norgett M J 1972 *Computational Solid State Physics* (New York: Plenum) p 385
- [41] Norgett M J 1972 *Atomic Energy Research Establishment Report AERE R7605*
- [42] Catlow C R A 1977 *Proc. R. Soc. A* **353** 533
- [43] Buckingham R A 1938 *Proc. R. Soc. A* **168** 264
- [44] Dick B G and Overhauser A W 1958 *Phys. Rev.* **112** 90
- [45] Kuklja M M and Pandey R 1999 *J. Am. Ceram. Soc.* **82** 2881
- [46] Lewis G V and Catlow C R A 1985 *J. Phys. C: Solid State Phys.* **18** 1149–61
- [47] Gale J D 1996 *Phil. Mag. B* **73** 3–19
- [48] Gale J D 1997 *J. Chem. Soc. Faraday Trans.* **93** 629
- [49] Bush T S, Gale J D, Catlow C R A and Battle P D 1994 *J. Mater. Chem.* **4** 831–7
- [50] Lewis G V and Catlow C R A 1986 *J. Phys. Chem. Solids* **47** 89–97
- [51] *Landolt–Börnstein New Series* 1969 Group III, vol 7 (Springer: Berlin)

- [52] Mott N F and Littleton M J 1938 *Trans. Faraday Soc.* **34** 485
- [53] Kröger F A and Vink H J 1956 *Sov. Solid State Phys.* vol 3 (New York: Academic)
- [54] Toolenaar F J C and de With G 1986 *Proc. Br. Ceram. Soc.* **37** 241–2
- [55] Mulder C A M and de With G 1985 *Solid State Ion.* **16** 87
- [56] Shimomura S and Nakazawa H 1993 *Inst. Phys. Conf. Ser.* **130** 579–82
- [57] Yamane H, Omori M, Okubo A and Hirai T 1993 *J. Am. Ceram. Soc.* **76** 2382–4
- [58] Catlow C R A, Gale J D and Grimes R W 1993 *J. Solid State Chem.* **106** 13–26
- [59] Cherry M, Islam M S and Catlow C R A 1995 *J. Solid State Chem.* **118** 125–32
- [60] Rotman S R and Tuller H L 1990 *Solid State Ion.* **40/41** 893–5
- [61] Rotman S R, Warde C, Tuller H L and Haggerty J 1989 *J. Appl. Phys.* **66** 3207
- [62] Lupei V, Lupei A and Boulon G 1996 *Phys. Rev. B* **53** 14 818
- [63] Donnerberg H and Catlow C R A 1994 *Phys. Rev. B* **50** 744
- [64] Kitaeva V F, Zharikov E V and Chisty I L 1985 *Phys. Status Solidi a* **92** 475–88
- [65] *Landolt–Börnstein* 1969 *New Series* Group III, vol 2, ed K-H Hellwege (Berlin: Springer)